Multi-Objective Optimization of High Torque Density Segmented PM Consequent Pole Flux Switching Machine with Flux Bridge

Wasiq Ullah, *Studnet member, IEEE*, Faisal Khan, *Member, IEEE*, and Muhammad Umair

***Abstract*— Due to double salient structure, Flux Switching Machines (FSMs) are preferred for brushless AC high speed applications. Permanent Magnet (PM) FSMs (PM-FSMs) are suited applicants where high torque density (T_{den}) and power density (P_{den}) are the utmost requisite. However conventional PM-FSMs utilizes excessive rare earth PM volume V_{PM}, higher cogging torque T_{cog}, high torque ripples (T_{rip}) and comparatively lower (T_{den}) and P_{den} due to flux leakage. To overcome the aforesaid demerits, a new high (T_{den}) Segmented PM Consequent Pole (CP) FSM (SPMCPFSM) with flux bridge and barrier is proposed which successfully reduces V_{PM} by 46.52% and PM cost by 46.48%. Moreover, Multi-Objective Optimization (MOO) examines electromagnetic performance due to variation in geometric parameters for global optimum parameters with key metric such as flux linkage (Φ_{pp}), flux harmonics (Φ_{THD}) average torque (T_{avg}), T_{cog}, T_{rip}, T_{den}, average power (P_{avg}) and P_{den}. Analysis reveals that MOO improve Φ_{pp} by 22.68%, boost T_{avg} by 11.41%, enhanced P_{avg} by 4.55% and increased T_{den} and P_{den} by 11.41%. Detailed electromagnetic performance comparison with existing state of the art shows that proposed SPMCPFSM offer T_{avg} maximum up to 88.8%, truncate T_{rip} up to 24.8%, suppress T_{cog} up to 22.74%, and results 2.45 times T_{den} and P_{den}.**

***Index Terms*— Consequent Pole, multi-objective optimization, finite element analysis, optimization, segmented PM, AC Machine.**

I. INTRODUCTION

FLUX Switching Machines (FSMs) are examples of stator active brushless AC machine in which all the excitations sources (Permanent Magnets, field winding slot and Armature winding slots) resides on stator leaving passive rotor made of iron only. Based on excitation source, FSMs are classified in to three major class i.e. Permanent Magnet (PM) excited, field excited and Hybrid excited (PM and field excited) [1]. The three major class of the FSMs are Permanent Magnet FSMs (PM-FSMs), Field Excited FSMs (FE-FSMs) and Hybrid Excited FSMs (HE-FSMs) which are further divided into outer rotor, inner rotor, dual rotor and dual stator and various stator structure as shown in Fig. 1. Among three major FSMs topologies, FE-FSM provide better flux controllability however offer low torque density. HE-FSM provide comparatively higher torque density however the stator design is highly complex due to exitance of both PM and field excitation. PM-FSMs provide higher torque density therefore considered for detail investigation.

Structural based, PM-FSMs are classified as partitioned stator, magnet shaping and stator shaping. In stator shaping, PMFSMs are classified in U-shape Module, Flux adjustor, E/C-Core, Multi-tooth, π- shape, V-shape and square envelope. The aforesaid structural variation in design of PM-FSMs are performed to achieve the higher torque density and reduce the PM usage, reduce machine cost, suppress machine weight, truncate machine volume, eliminate leakage flux and improve electromagnetic performance.

In the aforesaid topologies of PM-FSMs despite of high PM volume usage, U-shape modules are associated with stator leakage flux [2, 3]. Leakage flux is compensated with Mechanical Flux Adjustor (MFA) in all pole and alternate pole however, MFA entails additional mechanical equipment that rise machine mass, cost and volume [4, 5]. E/C-Core and multi-tooth reduce PM volume by increasing the slot area to improve electromagnetic performance [6-8] however, leakage flux issue is dominant from stator to surrounding and narrow flux modulation pole in multi-tooth get saturated. $\pi-$ shape improves electromagnetic performance [9] but despite of more PM usage and leakage flux, $\pi-$ shape stator assembling, and manufacturing is complex. V-shape is considered with electrical and mechanical loading at supportive base of V legs [10, 11]. The associated mechanical and electrical loading are overcome in square envelop however this design offered comparative lower torque density [12].

Stator leakage flux suppression has been a trending research area from the last decades which leads to the development of Consequent Pole (CP) structures in both stator and rotor PM-FSMs. In rotor PMs CP designs, author in [13] investigated presence of even order harmonics with unipolar leakage flux whereas it's comparison with hybrid pole PM and CP machines are presented in [14]. However, despite of mechanical constraints, effects of cogging torque and torque ripples are dominant which resulted pulsating instantaneous torque. Cogging torque and torque ripples are suppressed in [15] using various magnetic pole however in this technique, average torque reduced. Author [16] introduced spoke type rotor CP machine to maintain average torque but unfortunately core loss

Manuscript received June 05, 2020; revised August 31, 2020; accepted October 23, 2020. date of publication March 25, 2021; date of current version March 18, 2021.

Wasiq Ullah, Faisal Khan and Muhammad Umair are with the Department of Electrical and Computer Engineering, COMSATS University Islamabad, Abbottabad Campus, 22060, Pakistan. E-mails: (wasiqullah014@gmail.com, faisalkhan@cuiatd.edu.pk, muhammadumair1221@gmail.com)
(Corresponding Author: Ullah, Wasiq)

Digital Object Identifier 10.30941/CESTEMS.2021.00005

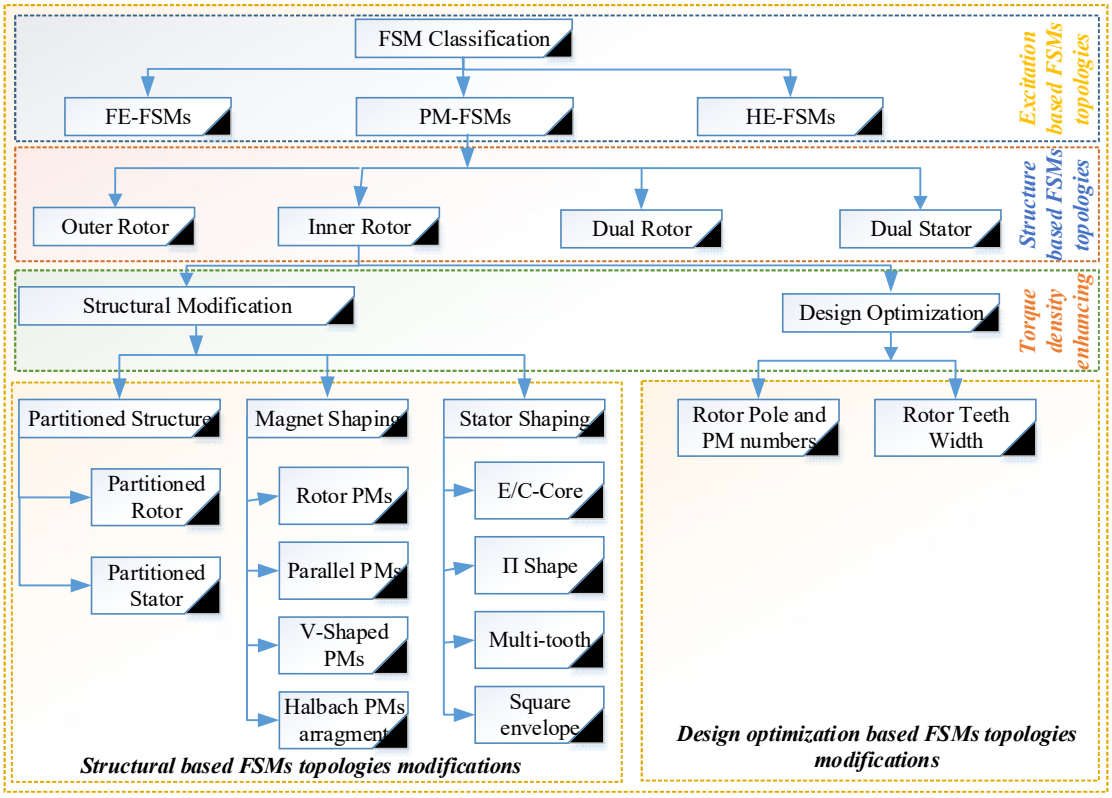

Fig. 1. General FSMs classification and structural variation of PM-FSMs topologies.

density increases, and irreversible demagnetization occur at the spoke type PM edge closer to air gap. Moreover, segmented PMs in rotor associated mechanical constraints.

Flux leakage from stator is successfully suppressed in CP PM-FSMs (CP-PM-FSMs) with flux barriers as shown in Fig. 2(a). This design effectively suppresses leakage flux from the stator end however utilizes large PM volume. Despite of more PM volume, the narrow flux barrier saturates which degrade electromagnetic performance. Moreover, the flux barrier offers short flux path that rise flux circulation and cancellation (exposed in Fig. 2(b)) which upsurge cogging torque and results pulsating torque and increases torque ripples. Furthermore, electromagnetic performances are degraded resulting reduction in torque and power densities [17].

The aforesaid design offer more PM volume utilization, PM cost, stator leakages flux, machine mass, flux circulation and cancellation linked with conventional PM-FSM and CP-PM-FSM, a new topology of 6S-13P (stator slot-rotor pole) Segmented PM CP FSM (SPMCPFSM) with reduced PM usage is proposed as shown in Fig. 3. Fig. 3(a), shows that proposed SPMCPFSM successfully lessen high PM volume utilization through stator pole alternative to PMs and truncated flux cancellation and circulation. Moreover, from Fig. 3(b) it can be clearly seen that SPMCPFSM at initial design stage successfully suppressed flux barrier saturation. In comparison with conventional PM-FSMs, SPMCPFSM exhibits lower torque ripple, cogging torque and higher torque and power densities.

Based on illustration in Fig.3, structural modification is successfully performed on PM shaping and stator shaping to achieve higher torque density SPMCPFSM. In order to further improve torque capability, the design is proceeded for optimization based on multi-variable techniques used for Multi-Objective Optimization (MOO). Various multi-objective optimization techniques have been formulated in different FSMs topologies [18-26] for enhancing electromagnetic performance, comparison of single-variable and multi-variable and design refinement to achieve global optimum parameters. Comparison of optimization techniques compel author for design refinement utilizing multi-objective optimization based on multi-variable geometric parameters. This technique has key advantage of enhancing overall electromagnetic performances.

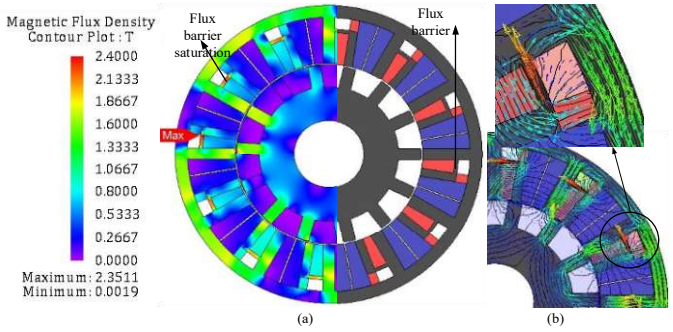

Fig. 2. Consequent Pole PM-FSM (a) Nephogram and cross-sectional view (b) Flux cancellation and circulation

Main contributions of this paper include designing of a new SPMCPFSM at 46.52% reduced PM volume that suppress the overall PM cost by 46.48 and enhancing the flux modulation phenomena for higher torque density. Furthermore, Multi-Objective Optimization (MOO) is opted for torque capability and achieving global optimum design parameters. Comprehensive performance analysis reveals that the

developed SPMCPFSM offer average torque maximum up to 88.8%, truncate torque ripples up to 24.8%, suppress cogging torque up to 22.74%, and boost torque and power density up to 2.45 times in comparison with state of the art.

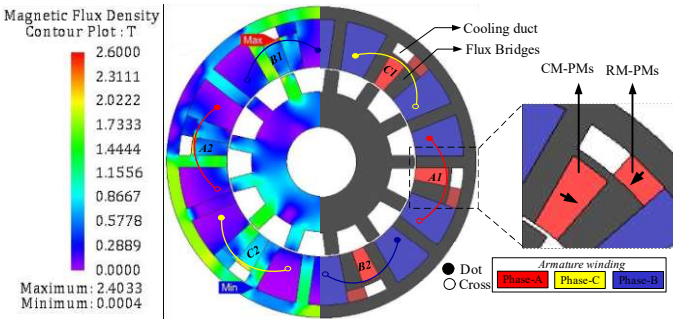

Fig. 3. Proposed SPMCPFSM cross sectional view, winding and PMs configuration

Overall paper is ordered as, section II describes SPMCPFSM construction, section III discuss multi-objective optimization, section IV compares initial and optimized SPMCPFSM design, section V compare proposed SPMCPFSM and conventional PM-FSMs topologies and finally, some conclusions are drawn in section VI.

II. SPMCPFSM Construction

The developed SPMCPFSM is designed based on the design parameters as listed in Table I and indicated in Fig 4. 2D cross sectional view in Fig. 3 shows that in SPMCPFSM, each winding phase of armature coils are composed of two coils set concentrated between segmented PMs with different magnetization pattern. The first PM segment lying in the lower part of the stator is Circumferentially Magnetized PMs (CM-PMs) whereas the 2nd segmented enclosed between flux bridge, flux barrier and stator are Radial Magnetized PMs (RM-PMs). Furthermore, CM-PMs are bounded in flux barriers and bridge. The flux bridge not only act as 2nd pole of the PMs but also provide magnetic path for the flux distribution and linkage. This PM segmentation greatly helps in enhancing flux modulation phenomena and reducing the total PM usage.

It can be clearly seen that both segmented PMs are enclosed in h-shaped stator teeth occupied which helps to eliminates stator leakages flux going across the stator thus, converting leakage flux to flux linkage. Due to PM segmentation, flux distribution and linkage though air-gap occurs from stator yoke as well as flux bridge (as shown in Fig. 6(a)). This superposition of flux improves flux modulation effects of both PMs to superimpose each other by through flux bridge and barriers and results higher magnetic flux density which ultimately improve torque production capability and h-shaped stator teeth with flux bridge and reduces PM slot effects to suppress cogging torque and torque ripples. In addition, h-shaped stator teeth provide cooling duct (as shown in Fig. 4) for heat flow to avoid PM demagnetization and overheating to ensure reduce temperature distribution. It is also worth mentioning that in comparison with conventional PM-FSMs, the flux modulation in SPMCPFSM not only occur through stator teeth but also with flux bridge (as shown in Fig. 5) which further improve overall flux circulation. This dual modulation phenomena in SPMCPFSM improves overall performance and results higher torque density and electromagnetic performance.

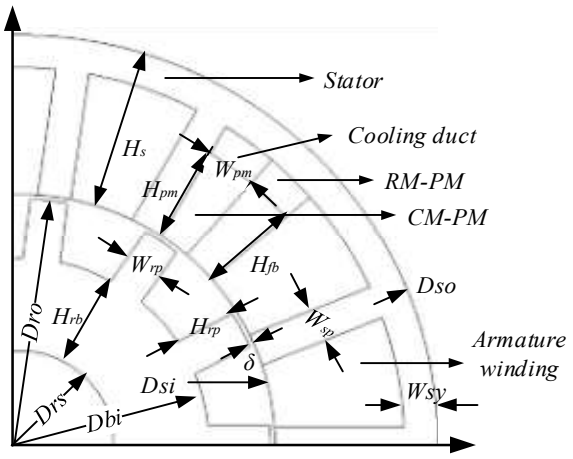

Fig. 4. Design parameters for construction of SPMCPFSM

TABLE I
DESIGN PARAMETERS OF SPMCPFSM

Symbol	Parameter	Value (mm)
W_{pm}	PM width	2.1
H_{pm}	PM height	9.5
H_{fb}	Flux barrier height	10.5
H_{rb}	Rotor back iron height	10.2
D_{ro}	Rotor outer radius	27
D_{si}	Stator inner radius	27.5
W_{rp}	Rotor pole width	4
H_{rp}	Rotor pole height	6.6
H_s	Stator height	17.5
W_{sy}	Stator yoke width	3.6
D_{rs}	Rotor shaft	10.2
D_{so}	Outer radius of stator	45
δ	Airgap length	0.5

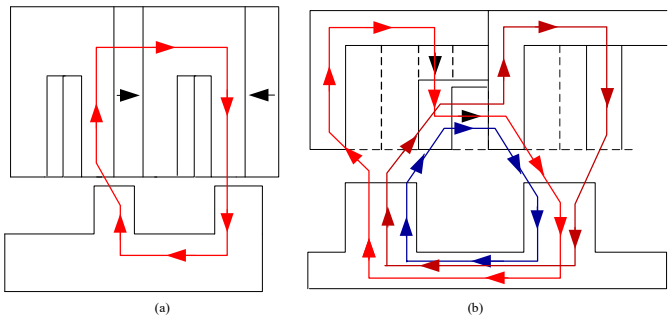

Fig. 5. Flux Modulation in (a) PM-FSMs (b) SPMCPFSM.

Since machine construction is symmetrical, the flux in each coil remain same resulting sinusoidal flux linkage from all four coils sets. From Fig. 6(a) and Fig. 6(c), it can be clearly seen that maximum flux linkages occur when the rotor poles are aligned to the right or left tooth of stator pole A1 at d-axis position respectively. Moreover, from Fig. 6(b) and Fig. 6(d), zero-flux linkage is obtained when rotor pole is symmetric to stator slot q-axis. Note that rotor change its position from Fig. 6(a) - Fig. 6(c) the flux linkage becomes bi-polar. A typical bi-polar flux linkage of one coil set over one periodic cycle is shown in Fig 7.

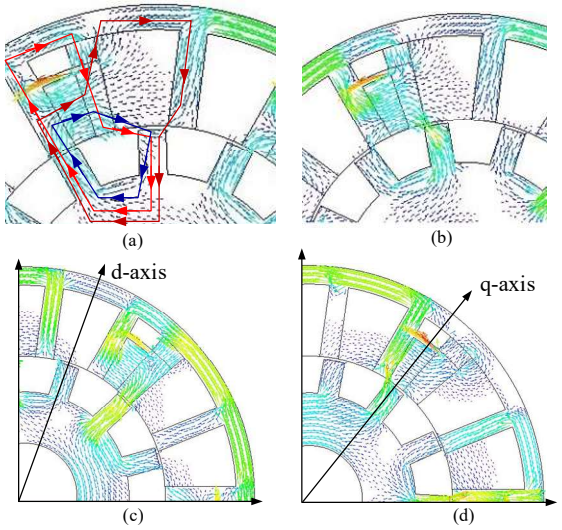

Fig. 6. Open-Circuit flux distribution of SPMCPFSM (a) Rotor at negative d-axis (b) Rotor at q-axis (c) Rotor at d-axis and (d) Rotor at negative q-axis

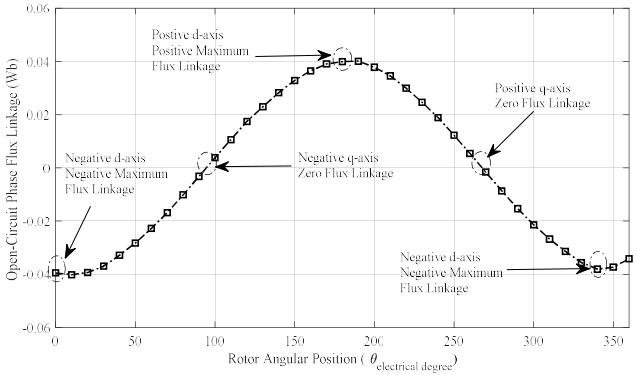

Fig. 7. Typical open-circuit phase flux linkage of SPMCPFSM in one periodic cycle

III. MULTI-OBJECTIVE OPTIMIZATION

As per classification of PM-FSMs, for higher torque density capability, structural modification is perfectly performed and proceeded to optimization based on MOO for global optimum design parameters and strengthen electromagnetic performance. MOO examines impact of main design geometry such as split ratio (β_s), H_{pm}, H_{fb} W_{rp}, W_{pm}, W_{fb} and H_{rp} with key matric such as flux linkage (Φ_{pp}), flux harmonics (Φ_{THD}), average torque (T_{avg}), cogging torque (T_{cog}), torque ripples (T_{rip}), torque density (T_{den}), average power (P_{avg}) and power density (P_{den}). Initial design electromagnetic performance is listed in Table II whereas MOO flow chart is shown in Fig. 8. During implementation of MOO, priority is set to select design offering highest torque density. MOO is applied to investigate effect of leading geometry parameters on performances of 6S-13P SPMCPFSM. For this purpose, MOO is implemented based on objective function, constrains, variable limits as expressed

$$\begin{cases} \textit{objective Function}: \\ \text{maxmize}\left(T_{avg}, T_{den}, P_{avg}, P_{den}\right) \\ \text{constraint}: T_{avg} \geq 3.81Nm,\ T_{den} \geq 470kNm/m^3 \\ P_{den} \geq 62kW/kg, P_{avg} \geq 940.95W \\ \textit{Variable set 1}: \left[\beta_s \quad H_{pm} \quad H_{fb} \quad W_{rp}\right] \\ \textit{Variable set 2}: \left[W_{rp} \quad W_{pm} \quad W_{fb} \quad H_{rp}\right] \end{cases} \tag{1}$$

$$\begin{cases} \textit{Variables limits}\left(\textit{upper/lower}\right) \\ \beta_s: \quad 0.55 \leq \beta_s \leq 0.65 \\ W_{rp}\left(mm\right): \quad 2.8 \leq W_{rp} \leq 4.6 \\ H_{pm}\left(mm\right): \quad 5.1 \leq H_{pm} \leq 10.1 \\ W_{pm}\left(mm\right): \quad 2.5 \leq W_{pm} \leq 5.0 \\ H_{fb}\left(mm\right): \quad 7.1 \leq H_{pm} \leq 10.1 \\ W_{fb}\left(mm\right): \quad 0 \leq W_{fb} \leq 1.0 \\ H_{rp}\left(mm\right): \quad 5.8 \leq H_{rp} \leq 7.4 \end{cases} \tag{2}$$

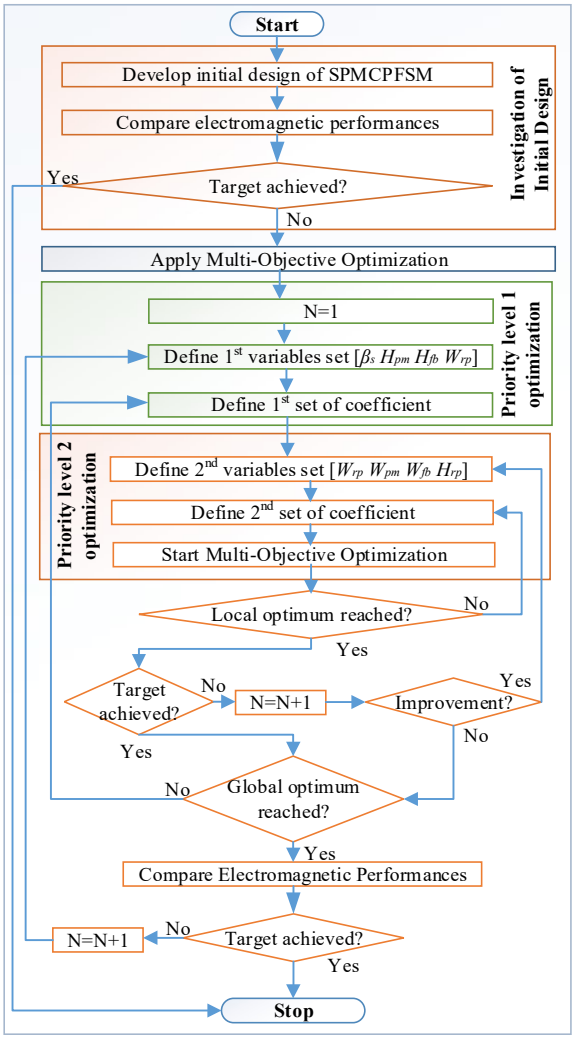

Fig. 8. Flow chart for Multi-Objective Optimization

The above said optimization variable limits are obtained utilizing optimization coefficient as

$$\beta_s = \frac{D_{si}}{D_{so}} \tag{3}$$

$$K_{H_{rp}} = \frac{H_{rp}}{H_{rp} + H_{rb}} \tag{4}$$

$$K_{pmH} = \frac{\Delta H_{pm}}{H_{pm}} \tag{5}$$

$$K_{pmW} = \frac{\Delta W_{pm}}{W_{pm}} \tag{6}$$

$$K_{fbH} = \frac{\Delta H_{fb}}{H_{fb}} \quad (7)$$

$$K_{fbW} = \frac{\Delta W_{fb}}{W_{fb}} \quad (8)$$

Overall MOO is applied on predefined optimization variables having defined boundary upper and lower limits in multiple iteration (N). During implementation of MOO, most sensitive variables is considered first followed by the rest in the same decreasing order of sensitivity. Since MOO is based on multi-variables, therefore, in each step two optimization variables are considered in one time such as β_s in company with W_{rp}, H_{pm} with W_{pm}, H_{fb} with W_{fb} and W_{rp} with H_{rp}.

In comparison of single variable optimization, multiples variables reduce computation time and results global optimum parameters. The above-mentioned eight geometric parameters can be solved in eight steps whereas here in multi-variable it is reduced to four steps at all. These optimization variables sequentially optimize stator and rotor for global optimum parameters. It is worth mentioning that during MOO, magnetic/electrical loading (PM volume. armature turns, current density), machine axial length, armature winding slot area and air gap dimension is fixed so that electromagnetic performance are purely due design parameters. Effect of geometric parameters on electromagnetic performance utilizing MOO are investigated in the proceeding sub-sections.

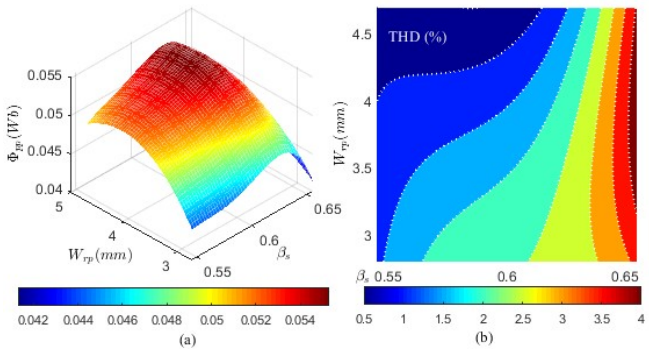

Fig. 9. Effect of β_s and W_{rp} optimization on flux (a) Φ_{pp} (b) Φ_{THD}

A. β_s and W_{rp} Optimization

β_s is the ratio of D_{si} and D_{so}. β_s and W_{rp} effect T_{avg} and Φ_{pp} respectively. During implementation of MOO, β_s is maintained in the range of $W_{sy}/2$ and W_{sy} to confirm uniform stator tooth magnetic field distribution and avoid W_{sy} saturation. Effect of this optimization parameters on flux, power and torque behaviors with the foregoing key performance indicators are shown in Fig. 9 to Fig. 11 respectively whereas electromagnetic performance of initial SPMCPFSM design with this step optimization (term as SPMCPFSM-1) are listed in table II.

Based on electromagnetic performances, analysis reveals that Φ_{pp} is improved by 2.8%, diminish Φ_{THD} by 12.3%, boost T_{avg} by 27.83%, truncate T_{rip} by 4.58%, enhanced P_{avg} by 3.26% and amplified T_{den} and P_{den} by 6.01% at the cost of 3.84% increase in T_{cog}. In this step of optimization both the

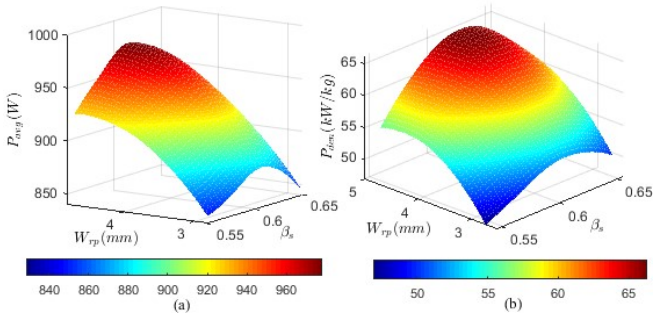

Fig. 10. Effect of β_s and W_{rp} optimization on power (a) P_{avg} (b) P_{den}

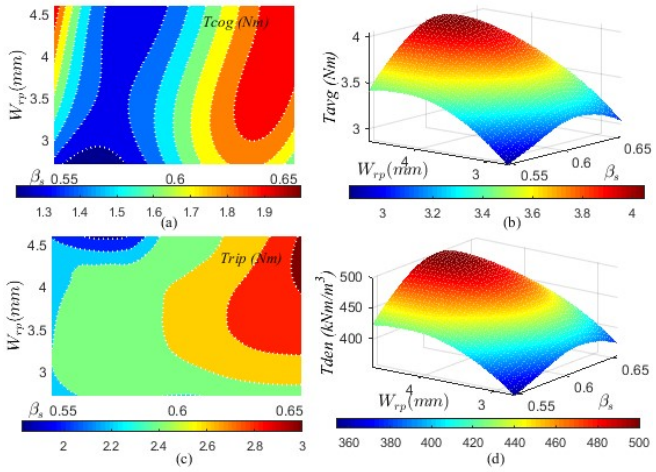

Fig. 11. Effect of β_s and W_{rp} optimization on torque profile (a) T_{cog} (b) T_{avg} (c) T_{rip} (d) T_{den}

TABLE. II
ELECTROMAGNETIC PERFORMANCE ANALYSIS WITH β_s AND W_{rp} OPTIMIZATION

Key performance indicator (unit)	SPMCPFSM	SPMCPFSM-1
Φ_{pp} (Wb)	0.0542143	0.0557807
Φ_{THD} (%)	2.2266795	1.952731
T_{cog} (Nm)	1.7629727	1.8307654
T_{avg} (Nm)	3.8178947	4.0476328
T_{rip} (Nm)	2.7251452	2.6002931
T_{den} (kNm/m^3)	471.85474	500.24815
P_{avg} (W)	941.6222	972.37134
P_{den} (kW/kg)	62.497317	66.258033

values of β_s and W_{rp} are updated from 0.61 and 3.6 mm to 0.62 and 4.4 mm respectively.

B. H_{pm} and W_{pm} Optimization

SPMCPFSM is developed utilizing partitioned Neodymium iron boron (NdFeB, Neomax-35AH) PMs with two segments with different magnetization pattern with +220 °C recommended temperature. This optimization step investigates H_{pm} and W_{pm} of CM-PMs. For this purpose, H_{pm} limits are defined as 5.1 mm to 10.1 mm whereas W_{pm} are defined between 2.5 mm to 5.0 mm. Note that in variation of H_{pm} and W_{pm} the PM volume are kept constant by varying H_{pm} and W_{pm} of RM-PMs. Furthermore, variation of W_{pm} is adjusted with adjacent flux barriers span. Fig. 12 to Fig. 14

shows variation of electromagnetic performance i.e. flux, torque and power with CM-PMs H_{pm} and W_{pm} whereas electromagnetic performance of this step optimization (term as SPMCPFSM-2) are listed in table III.

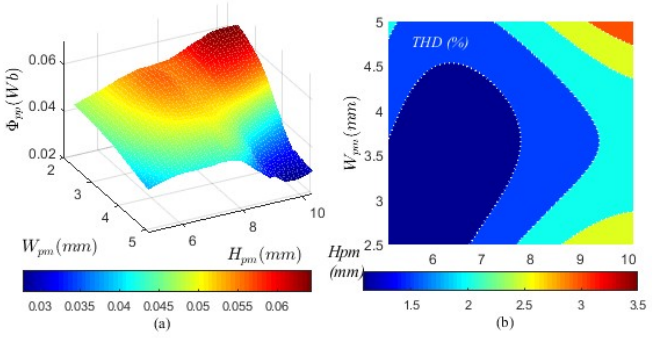

Fig. 12. Effect of H_{pm} and W_{pm} optimization on flux (a) Φ_{pp} (b) Φ_{THD}

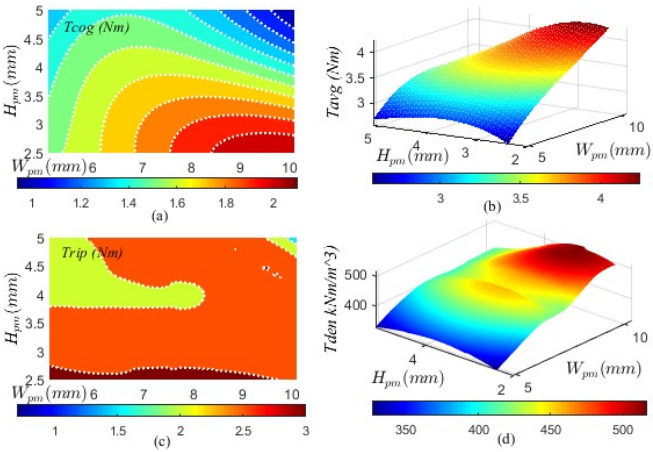

Fig. 13. Effect of H_{pm} and W_{pm} optimization on torque profile (a) T_{cog} (b) T_{avg} (c) T_{rip} (d) T_{den}

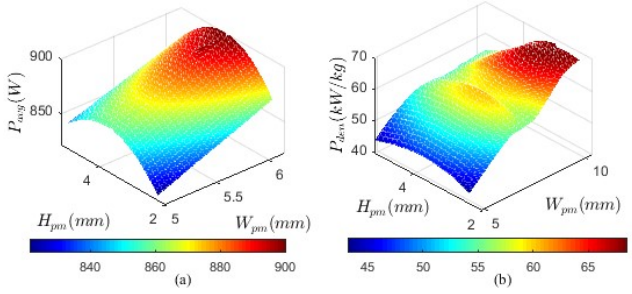

Fig. 14. Effect of H_{pm} and W_{pm} optimization on power (a) P_{avg} (b) P_{den}

TABLE. III
ELECTROMAGNETIC PERFORMANCE ANALYSIS WITH H_{pm} AND W_{pm} OPTIMIZATION

Key performance indicator (unit)	SPMCPFSM-1	SPMCPFSM-2
Φ_{pp} (Wb)	0.0557807	0.063774
Φ_{THD} (%)	1.952731	2.830655
T_{cog} (Nm)	1.8307654	2.0598425
T_{avg} (Nm)	4.0476328	4.1527403
T_{rip} (Nm)	2.6002931	2.9375029
T_{den} (kNm/m^3)	500.24815	501.24891
P_{avg} (W)	972.37134	973.35896
P_{den} (kW/kg)	66.258033	67.728333

Electromagnetic performances unveil that Φ_{pp} is enhanced by 14.32%, improved T_{avg} by 2.59%, increase P_{avg} by 0.101% and improve T_{den} and P_{den} by 0.2485%. In this step of optimization both the values of H_{pm} and W_{pm} are updated from 8.1 mm and 3.5 mm to 9.1 mm and 3.0 mm respectively.

C. H_{fb} and W_{fb} Optimization

The developed SPMCPFSM encloses h-shaped stator encompassing CM-PMs and RM-PMs in flux bridge to alter magnetic field distribution and provide path for working harmonics of the magnetic field distribution to improve flux modulation process. However, flux barriers results leakage flux due to flux circulation the in the stator yoke through RM-PMs. The flux barrier width (W_{fb}) in initial design is set to be 1 mm but undergo saturation therefore, to investigates the optimum W_{fb} and H_{fb} this optimization step is proceeded. It is worth mentioning that H_{fb} is the same as flux bridge height and the optimized parameter for both will be same. This step reduces one step optimization process and reduces computational time further. Detailed electromagnetic performance analysis of flux, torque and power with H_{fb} and W_{fb} are shown in Fig. 15 to Fig. 17 whereas electromagnetic performance of (term as SPMCPFSM-3) are listed in table IV.

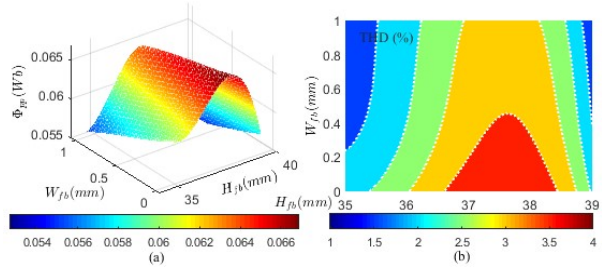

Fig. 15. Effect of H_{fb} and W_{fb} optimization on flux (a) Φ_{pp} (b) Φ_{THD}

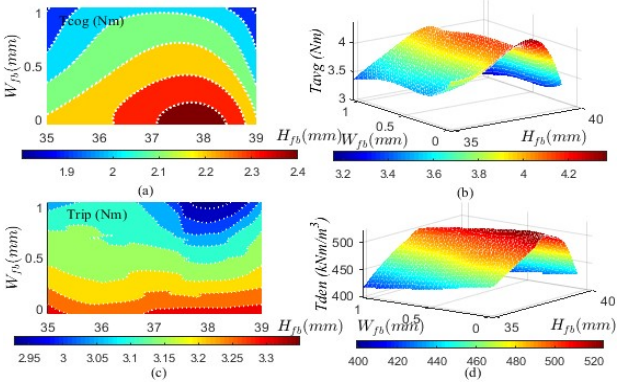

Fig. 16. Effect of H_{fb} and W_{fb} optimization on torque profile (a) T_{cog} (b) T_{avg} (c) T_{rip} (d) T_{den}

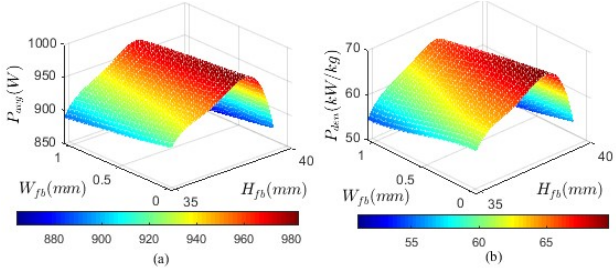

Fig. 17. Effect of H_{fb} and W_{fb} optimization on power (a) P_{avg} (b) P_{den}

TABLE. IV
ELECTROMAGNETIC PERFORMANCE ANALYSIS WITH H_{fb} and W_{fb} OPTIMIZATION

Key performance indicator (unit)	SPMCPFSM-2	SPMCPFSM-3
Φ_{pp} (Wb)	0.063774	0.0663154
Φ_{THD} (%)	2.830655	4.0204716
T_{cog} (Nm)	2.0598425	2.4396466
T_{avg} (Nm)	4.1527403	4.2491503
T_{rip} (Nm)	2.9375029	3.305396
T_{den} (kNm/m^3)	501.24891	525.15376
P_{avg} (W)	973.35896	981.98522
P_{den} (kW/kg)	67.728333	69.556789

Quantitative electromagnetic performances reveal that H_{fb} shows slight sensitivity to variation in overall performance with dominancy on T_{avg} that ultimately improve P_{den} . It can be clearly seen that Φ_{pp} is increased by 3.98%, enhanced T_{avg} by 2.32%, improve P_{avg} by 0.88% and improve T_{den} and P_{den} by 4.76%. In this step of optimization both the values of H_{fb} and W_{fb} are updated from 10.5 mm and 3.83 mm to 10.1 mm and 4.8 mm respectively.

D. W_{rp} and H_{rp} Optimization

Once stator parameters are optimized for global optimum points, now rotor is optimized. Two major influencing parameters of rotor i.e. W_{rp} and H_{rp} are selected for optimization. Since, W_{rp} is optimized earlier, at this stage very fine variation are taken for consideration to reaches the best optimum solution. Variation of the electromagnetic performance i.e. flux; torque and power are shown in Fig. 18 to Fig. 20 whereas quantitative electromagnetic performance of (term as SPMCPFSM-4) are listed in table V.

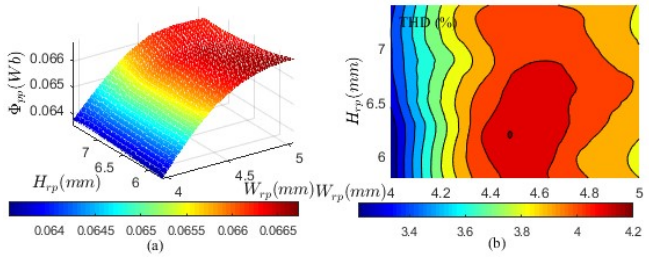

Fig. 18. Effect of W_{rp} and H_{rp} optimization on flux (a) Φ_{pp} (b) Φ_{THD}

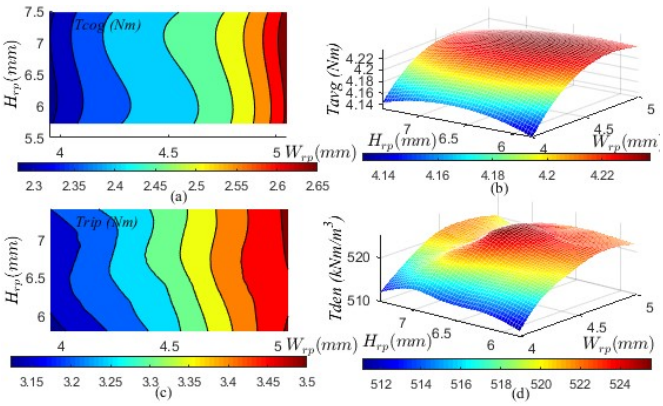

Fig. 19. Effect of W_{rp} and H_{rp} optimization on torque profile (a) T_{cog} (b) T_{avg} (c) T_{rip} (d) T_{den}

TABLE. V
ELECTROMAGNETIC PERFORMANCE ANALYSIS WITH W_{rp} AND H_{rp} OPTIMIZATION

Key performance indicator (unit)	SPMCPFSM-3	SPMCPFSM-4
Φ_{pp} (Wb)	0.0663154	0.0665131
Φ_{THD} (%)	4.0204716	4.223629
T_{cog} (Nm)	2.4396466	2.4846746
T_{avg} (Nm)	4.2491503	4.2536893
T_{rip} (Nm)	3.305396	3.340498
T_{den} (kNm/m^3)	525.15376	525.71473
P_{avg} (W)	981.98522	984.53276
P_{den} (kW/kg)	69.556789	69.63109

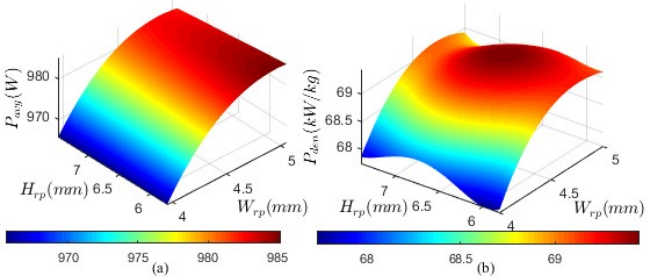

Fig. 20. Effect of W_{rp} *and* H_{rp} optimization on power (a) P_{avg} (b) P_{den}

Quantitative electromagnetic performances reveal that both W_{rp} *and* H_{rp} shows least sensitivity to variation in overall electromagnetic performance whereas only W_{rp} shows sensitivity to flux linkage because with the increase in W_{rp} the pole changes from un-aligned position to aligned position causing maximum flux linkage. Analysis shows that Φ_{pp} is increased by 0.29%, enhanced T_{avg} by 0.10%, improve P_{avg} by 0.255% and improve T_{den} and P_{den} by 0.10%. In this step of optimization both the values of W_{rp} and H_{rp} are updated from 4.4 mm and 6.8 mm to 4.6 mm and 6.6 mm respectively. This optimization step confirms that stator parameters are the major key influencing parameters in design of SPMCPFSM.

IV. COMPARISON OF INITIAL AND OPTIMIZED SPMCPFSM DESIGN

In order to visualize influence of MOO on electromagnetic performance as well geometric parameters, both initial and optimized parameters are investigated discussed in this stage. For comparison, both initial and optimized performance are listed in table VI and shown in Fig. 21 to Fig. 24.

Based on electromagnetic performances, analysis reveals that Φ_{pp} is improved by 22.68%, boost T_{avg} by 11.41%, enhanced P_{avg} by 4.55% and increased T_{den} and P_{den} by 11.41% at the cost of increase in T_{cog} , T_{rip} and Φ_{THD} which are reduced utilizing harmonic injection in [30].

Based on MOO, initial and optimized design parameters obtained are recorded in table VII whereas initial and optimized design are shown in Fig. 25 and flux distribution in Fig. 26. In comparison with initial design, it can be seen that optimized design suppressed inter slot flux flow.

Moreover, the final optimized model is investigated under wide range current densities and applied current angle for the torque/power versus speed curve and operating current phase for torque profile as shown in Fig. 27 and Fig. 28. In Fig. 27, power slightly decrease with speed due to increases in iron losses. Therefore, at higher speed (14000 r/sec) output power is dropped from 1200 Watt to 400 Watt (66.66%).

TABLE. VI
ELECTROMAGNETIC PERFORMANCE ANALYSIS OF INITIAL AND OPTIMIZED SPMCPFSM

Key performance indicator (unit)	Initial design	Optimized design
Φ_{pp} (Wb)	0.0542143	0.0665131
Φ_{THD} (%)	2.2266795	4.223629
T_{cog} (Nm)	1.7629727	2.4846746
T_{avg} (Nm)	3.8178947	4.2536893
T_{rip} (Nm)	2.7251452	3.340498
T_{den} (kNm/m^3)	471.85474	525.71473
P_{avg} (W)	941.6222	984.53276
P_{den} (kW/kg)	62.497317	69.63109

TABLE. VII
INITIAL AND OPTIMIZED DESIGN PARAMETERS

Parameter	Initial value	Optimized value
β_s	0.61	0.62
H_{pm}	8.1	9.1
W_{pm}	3.5	3
H_{fb}	10.5	10.1
W_{fb}	3.83	4.8
W_{rp}	4.4	4.6
H_{rp}	6.8	6.6

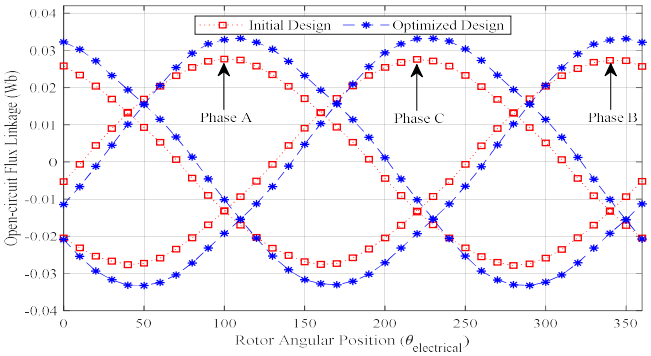

Fig. 21. Open-Circuit flux linkage comparison

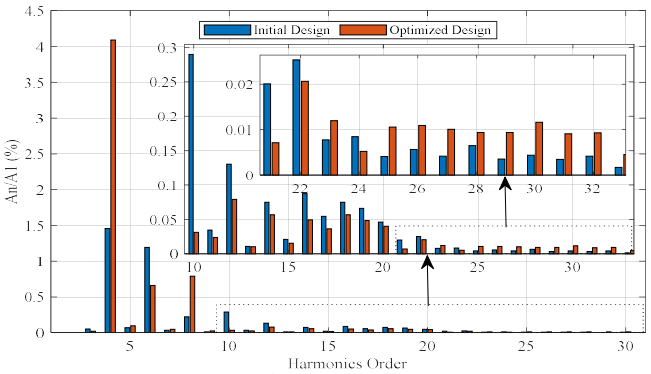

Fig. 22. Harmonics content of flux linkage

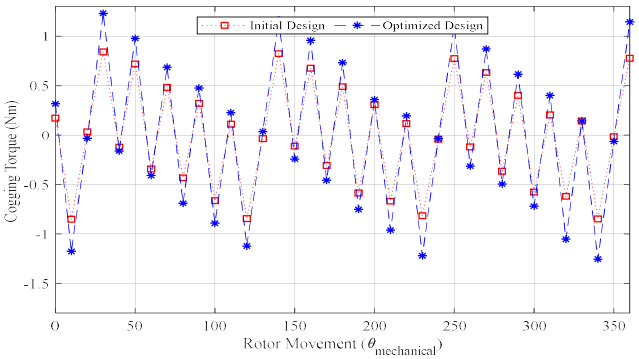

Fig. 23. Cogging torque of initial and optimized SPMCPFSM

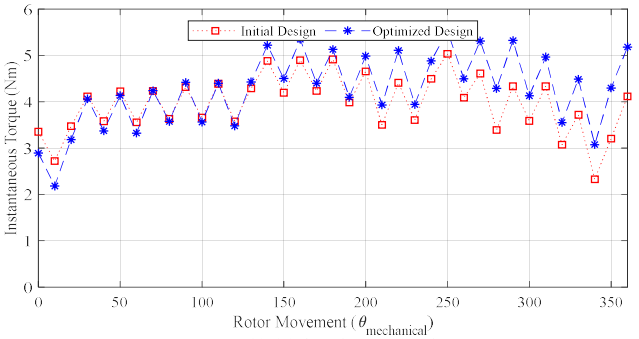

Fig. 24. Instantaneous torque of initial and optimized SPMCPFSM

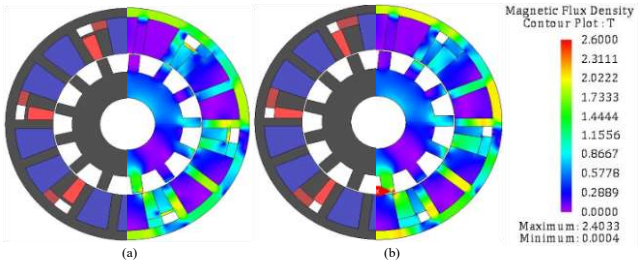

Fig. 25. Cross sectional view of (a) Initial SPMCPFSM design and (b) Optimized SPMCPFSM design

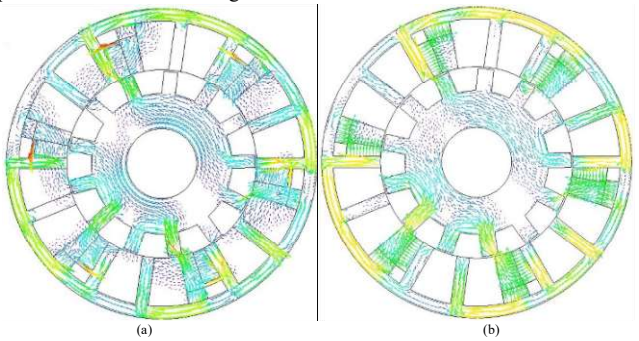

Fig. 26. Flux distribution of (a) Initial SPMCPFSM design and (b) Optimized SPMCPFSM design

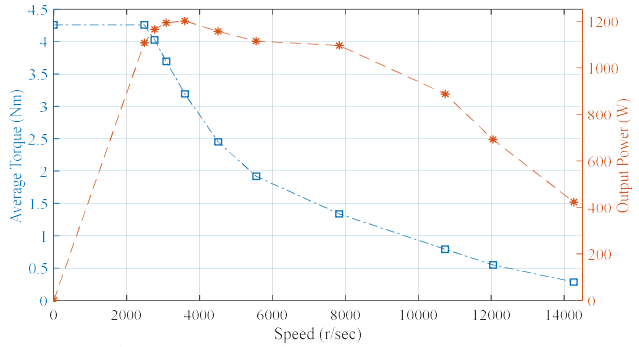

Fig. 27. Torque/power verses speed curve of SPMCPFSM

TABLE. VIII
QUANTITATIVE ELECTROMAGNETIC PERFORMANCE COMPARISON OF PROPOSED SPMCPFSM AND CONVENTIONAL PM-FSM AND CP-PM-FSMS TOPOLOGIES

Key performance indicator (unit)	SPMCPFSM Topologies		E-Core PM-FSMs		C-Core PM-FSMs	CP-PM-FSMs
	6S-13P	12S-13P	12S-10P	6S-10P	6S-10P	12S-14P
T_{avg} (Nm)	4.253	3.49	2.25	3.83	3.2	3.80
T_{cog} (Nm)	2.484	1.83	3.21	3.25	2.66	3.22
T_{rip} (Nm)	3.340	2.91	3.87	3.23	2.54	3.65
T_{den} (kNm/m^3)	525.714	431.83	214.35	364.93	304.96	321.33
P_{den} (kW/kg)	69.631	57.19	28.39	48.33	40.39	42.56
V_{PM} (mm^3)	8091.25			10505.75		11856.55
P_{PM} cos$t$ (s)	9.10			11.81		13.33

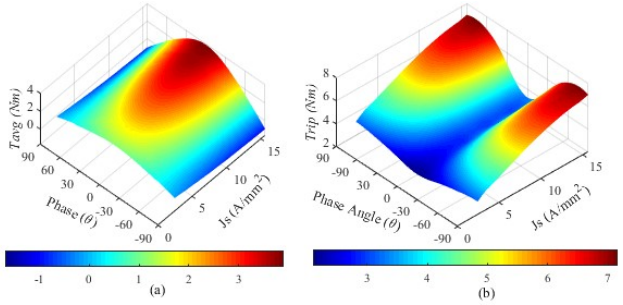

Fig. 28. Torque profile of (a) T_{avg} and (b) T_{rip}

V. COMPARISON OF PROPOSED SPMCPFSM AND CONVENTIONAL PM-FSMS TOPOLOGIES

The effectiveness of proposed 6S-13P is validated by comparing it with various state of the art such as 12S-13P SPMCPFSM [27-29], E/C-core PM-FSMs and CP-PM-FSMs with key performance indicators i.e. T_{cog}, T_{avg}, T_{rip}, T_{den}, and P_{den}, PM volume V_{PM} and PM cost. Aforesaid conventional designs are taken for comparison with proposed design. Extensive electromagnetic performance analysis of proposed SPMCPFSMs topologies and conventional E/C-core PM-FSMs and CP-PM-FSMs are listed in table VIII. It is worth mentioning that, for fair comparison of conventional and proposed SPMCPFSM design, air-gap diameter (0.5 mm), current density (15 A/mm^2), slot filling factor (0.5), stator outer diameter (45 mm), number of turns (180), stator/rotor core material (35H210), PM material (Neomax 35AH210 - NdFeB), stack length (25 mm), PM remanence (1.2 T) and PM relative Permeability (1.05) are kept constant. Moreover, optimized conventional designs are taken from literature [6, 7, 17] for comparison purpose whereas proposed SPMCPFSM is optimized in this paper for final comparison to show effectiveness of proposed model over various existing state of the art.

Comparison with E-Core 12S-10P PM-FSM reveals that 6S-13P SPMCPFSM exhibits 88.8% more T_{avg}, truncate T_{rip} by 14.7%, suppress T_{cog} by 22.74% with 2.45 times T_{den} and P_{den} whereas 12S-13P SPMCPFSM improve T_{avg} by 55.1%, reduces V_{PM} by 29.84%, PM cost by 29.78%, curtailed T_{rip} by 9.91%, reduces T_{cog} by 42.9% with 2.01 times T_{den} and P_{den}.

Comparison with E-Core 6S-10P PM-FSM illustrate that proposed 6S-13P SPMCPFSM design enhanced T_{avg} by 10.96%, decreases T_{cog} by 23.69%, suppress V_{PM} by 29.84%, PM cost by 29.78%, with 1.44 times T_{den} and P_{den} at the cost of 2.16% increase in T_{rip} whereas proposed 12S-13P reduces T_{avg} by 8.87%, lessen T_{avg} by 24.8%, reduces T_{cog} by 43.69% with 1.18 times T_{den} and P_{den}

Comparison with C-Core 6S-10P PM-FSM shows that proposed SPMCPFSM design enhanced T_{avg} by 32.81%, decrease T_{cog} by 6.76% with 1.72 times T_{den} and P_{den} at the cost of 29.9% increase in the T_{rip}. Whereas proposed 12S-13P improve T_{avg} by 9.06%, truncate T_{rip} by 14.56%, reduces T_{cog} by 31.2%, reduces V_{PM} by 29.84%, PM cost by 29.78%, with 1.41 times T_{den} and P_{den}.

Comparison with 12S-14P CP-PM-FSM reveals that 6S-13P SPMCPFSM design amplify T_{avg} by 11.84%, shrink T_{cog} by 22.96%, diminish T_{rip} by 9.58%, reduces V_{PM} by 46.52%, PM cost by 31.73%, with 1.63 times T_{den} and P_{den}. Whereas proposed 12S-13P offer 8.15% lower T_{avg}, curtailed T_{rip} by 14.56%, reduces T_{cog} by 43.16% and with 1.34 times T_{den} and P_{den}.

Detailed comparison with conventional state of the art including various topologies of PM-FSMs and CP-PM-FSMs reveals that proposed E-Core 6S-13P SPMCPFSM exhibits T_{avg} maximum up to 88.8%, suppressed T_{rip} up to 24.8%, suppress T_{cog} up to 22.74%, V_{PM} by 46.52%, PM cost by 46.48% and 2.45 times T_{den} and P_{den}.

VI. CONCLUSION

This paper proposed and investigates 6S-13P SPMCPFSM with flux bridge at reduce PM usage and PM cost. Moreover, MOO is preferred for investigating variation of electromagnetic performance with leading design parameters. Analysis unveil that MOO improve electromagnetic performance and amplified

torque and power densities. Comparison of proposed design with conventional state of the art shows that proposed SPMCPFSM offer higher average torque and results 2.45 times torque and power densities. Thus, it is concluded that proposed design is preferred when high torque and power densities are primal requirement and MOO is opted for electromagnetic performance due to design parameters.

REFERENCES

[1] Ullah, Wasiq; Khan, Faisal; Umair, Muhammad. "Sub-Domain Modelling and Multi-Variable Optimization of Partitioned PM Consequent Pole Flux Switching Machines", *IET Electric Power Applications,* vol. 14, no. 8, pp. 1360-1369, 2020.

[2] N. Ullah, F. Khan, W. Ullah, A. Basit, M. Umair, Z. Khattak, "Analytical Modelling of Open-Circuit Flux Linkage, Cogging Torque and Electromagnetic Torque for Design of Switched Flux Permanent Magnet Machine," *Journal of Magnetics,* vol. 23, no. 2, pp. 253-266, 2018.

[3] N. Ullah, F. Khan, W. Ullah, M. Umair and Z. Khattak, "Magnetic equivalent circuit models using global reluctance networks methodology for design of permanent magnet flux switching machine," in *Proc. of 2018 15th International Bhurban Conference on Applied Sciences and Technology (IBCAST),* Islamabad, 2018, pp. 397-404.

[4] R. Owen, Z. Q. Zhu, J. B. Wang, D. A. Stone and I. Urquhart, "Mechanically adjusted variable-flux concept for switched flux permanent-magnet machines," in *Proc. of 2011 International Conference on Electrical Machines and Systems,* Beijing, 2011, pp. 1-6

[5] Z. Q. Zhu, M. M. J. Al-ani, X. Liu, M. Hasegawa, A. Pride and R. Deodhar, "Comparison of alternate mechanically adjusted variable flux switched flux permanent magnet machines," in *Proc. of 2012 IEEE Energy Conversion Congress and Exposition (ECCE),* Raleigh, NC, 2012, pp. 3655-3662.

[6] Z. Q. Zhu and J. T. Chen, "Advanced Flux-Switching Permanent Magnet Brushless Machines," *IEEE Transactions on Magnetics,* vol. 46, no. 6, pp. 1447-1453, June 2010.

[7] J.T. Chen, Z.Q. Zhu, S. Iwasaki et al., "A novel E-core switched-flux PM brushless AC machine", *IEEE Trans. Ind. Appl.,* vol. 47, no. 3, pp. 1273-1282, 2011.

[8] Z. Q. Zhu, J. T. Chen, Y. Pang, D. Howe, S. Iwasaki and R. Deodhar, "Analysis of a Novel Multi-Tooth Flux-Switching PM Brushless AC Machine for High Torque Direct-Drive Applications," *IEEE Transactions on Magnetics,* vol. 44, no. 11, pp. 4313-4316, Nov. 2008.

[9] Y. Du, C. Zhang, X. Zhu, F. Xiao, Y. Sun, Y. Zuo, L. Quan., "Principle and analysis of doubly salient PM motor with π-shaped stator iron core segments," *IEEE Trans. Ind. Electron.,* vol. 66, no. 3, pp. 1962–1972, Mar. 2019.

[10] G. Zhao and W. Hua, "A novel flux-switching permanent magnet machine with v-shaped magnets," *AIP Adv.,* vol. 7, no. 5, pp. 056655/5, Feb. 2017.

[11] G. Zhao and W. Hua, "Comparative Study Between a Novel Multi-Tooth and a V-Shaped Flux-Switching Permanent Magnet Machines," *IEEE Transactions on Magnetics,* vol. 55, no. 7, pp. 1-8, July 2019, Art no. 8104908.

[12] L. Zhang, L. J. Wu, X. Huang, Y. Fang and Q. Lu, "A Novel Structure of Doubly Salient Permanent Magnet Machine in Square Envelope," *IEEE Transactions on Magnetics,* vol. 55, no. 6, pp. 1-5, June 2019.

[13] J. Li, K. Wang, F. Li, S. S. Zhu and C. Liu, "Elimination of Even-Order Harmonics and Unipolar Leakage Flux in Consequent-Pole PM Machines by Employing N-S-Iron–S-N-Iron Rotor," *IEEE Trans. on Ind. Electronics,* vol. 66, no. 3, pp. 1736-1747, March 2019.

[14] J. Li, K. Wang and C. Liu, "Comparative Study of Consequent-Pole and Hybrid-Pole Permanent Magnet Machines," *IEEE Trans on Energy Conversion,* vol. 34, no. 2, pp. 701-711, June 2019.

[15] F. Li, K. Wang, H. Sun and J. Kong, "Influence of Various Magnetic Pole on Electromagnetic Performance of Consequent-Pole Permanent Magnet Machine," *IEEE Access,* vol. 7, pp. 121853-121862, 2019.

[16] J. Li and K. Wang, "A Novel Spoke-Type PM Machine Employing Asymmetric Modular Consequent-Pole Rotor," *IEEE/ASME Transactions on Mechatronics,* vol. 24, no. 5, pp. 2182-2192, Oct. 2019.

[17] Y. Gao, D. Li, R. Qu, H. Fang, H. Ding and L. Jing, "Analysis of a Novel Consequent-Pole Flux Switching Permanent Magnet Machine with Flux Bridges in Stator Core," *IEEE Trans. on Energy Conversion,* vol. 33, no. 4, pp. 2153-2162, Dec. 2018.

[18] J. Le Besnerais, V. Lanfranchi, M. Hecquet and P. Brochet, "Multiobjective Optimization of Induction Machines Including Mixed Variables and Noise Minimization," *IEEE Transactions on Magnetics,* vol. 44, no. 6, pp. 1102-1105, June 2008.

[19] D. Lim, D. Woo, H. Yeo, S. Jung, J. Ro and H. Jung, "A Novel Surrogate-Assisted Multi-Objective Optimization Algorithm for an Electromagnetic Machine Design," *IEEE Transactions on Magnetics,* vol. 51, no. 3, pp. 1-4, March 2015, Art no. 8200804.

[20] U. B. Akuru and M. J. Kamper, "Formulation and Multiobjective Design Optimization of Wound-Field Flux Switching Machines for Wind Energy Drives," *IEEE Transactions on Industrial Electronics,* vol. 65, no. 2, pp. 1828-1836, Feb. 2018.

[21] Z. Xiang, X. Zhu, L. Quan and D. Fan, "Optimization design and analysis of a hybrid permanent magnet flux-switching motor with compound rotor configuration," *CES Transactions on Electrical Machines and Systems,* vol. 2, no. 2, pp. 200-206, June 2018.

[22] H. Chen, X. Liu, N. A. O. Demerdash, A. M. EL-Refaie, J. Zhao and J. He, "Comparison and Design Optimization of a Five-Phase Flux-Switching PM Machine for In-Wheel Traction Applications," *IEEE Transactions on Energy Conversion,* vol. 34, no. 4, pp. 1805-1817, Dec. 2019.

[23] W. Yan et al., "Design and multi-objective optimisation of switched reluctance machine with iron loss," *IET Electric Power Applications,* vol. 13, no. 4, pp. 435-444, 4 2019.

[24] X. Zhu, D. Fan, L. Mo, Y. Chen and L. Quan, "Multiobjective Optimization Design of a Double-Rotor Flux-Switching Permanent Magnet Machine Considering Multimode Operation," *IEEE Transactions on Industrial Electronics,* vol. 66, no. 1, pp. 641-653, Jan. 2019.

[25] J. Yu and C. Liu, "Multi-Objective Optimization of a Double-Stator Hybrid-Excited Flux-Switching Permanent-Magnet Machine," *IEEE Transactions on Energy Conversion,* vol. 35, no. 1, pp. 312-323, March 2020.

[26] Z. Q. Zhu and X. Liu, "Individual and global optimization of switched flux permanent magnet motors," in *Proc. of 2011 International Conference on Electrical Machines and Systems,* Beijing, 2011, pp. 1-6.

[27] Ullah, Wasiq; Khan, Faisal; Sulaiman, Erwan; Umair, Muhammad; Ullah, Noman; Khan, Bakhtiar: 'Analytical validation of novel consequent pole E-core stator permanent magnet flux switching machine', *IET Electric Power Applications,* vol. 14, no. 5, pp. 789-796, 2020.

[28] W. Ullah, F. Khan, N. Ullah, M. Umair, B. Khan and H. A. Khan, "Comparative Study Between C-Core/E-Core SFPMM with Consequent Pole SFPMM," in *Proc. of 2019 International Symposium on Recent Advances in Electrical Engineering (RAEE)*, Islamabad, Pakistan, 2019, pp. 1-6.

[29] W. Ullah, F. Khan, E. Sulaiman, M. Umair, N. Ullah and B. Khan, "Influence of Various Rotor Pole on Electromagnetic Performance of Consequent Pole Switched Flux Permanent Magnet Machine," in *Proc. of 2019 International Conference on Electrical, Communication, and Computer Engineering (ICECCE)*, Swat, Pakistan, 2019, pp. 1-6.

[30] W. Ullah, F. Khan, E. Sulaiman and M. Umair, "Torque characteristics of high torque density partitioned PM consequent pole flux switching machines with flux barriers," *CES Transactions on Electrical Machines and Systems*, vol. 4, no. 2, pp. 130-141, June 2020.

Wasiq Ullah is basically from Afghanistan and was born in District Peshawar, Khyber Pakhtunkhwa, Pakistan in 1995. He received his B.S. and M.S degrees in electrical (power) engineering from COMSATS University Islamabad (Abbottabad Campus), Abbottabad, Pakistan in 2018 and 2020, respectively. He is currently pursuing PhD degree in electrical (power) engineering from COMSATS

University Islamabad (Abbottabad Campus), Abbottabad, Pakistan.

From 2018 till now, he is Research Associates with Electric Machine Design research group. His research interests include analytical modelling, design analysis and optimization of Permanent Magnet Flux Switching Machines, Linear Flux Switching Machines, Hybrid Excited Flux Switching Machines and novel Consequent pole Flux Switching Machines for high-speed brushless AC applications.

Faisal Khan was born in District Charsada, Khyber Pakhtunkhwa, Pakistan in 1986. He received the B.S. degree in electronics engineering from COMSATS University Islamabad (Abbottabad Campus), Pakistan in 2009 and M.S. degree in electrical engineering from COMSATS University Islamabad (Abbottabad Campus), Pakistan in 2012. He received the Ph.D. degree in electrical engineering from Universiti Tun Hussein Onn Malaysia, Malaysia in 2017.

From 2010 to 2012, he was a Lecturer at University of Engineering & Technology, Abbottabad, Pakistan. Since 2017, he has been Assistant Professor with the Electrical Engineering Department, COMSATS University Islamabad (Abbottabad Campus), Pakistan. He is author of more than seventy publications, one patent, and received multiple research awards. His research interests include design of flux-switching, synchronous, and dc machines.

Muhammad Umair was born in District Peshawar, Khyber Pakhtunkhwa, Pakistan in 1995. He received B.S. degrees in electrical (power) engineering COMSATS University Islamabad (Abbottabad Campus), Abbottabad, Pakistan in 2018. He is currently perusing M.S degree in Electrical (Power) Engineering at COMSATS University Islamabad (Abbottabad Campus). His research interests include design, analysis, optimization and experimental validation of electrical excited flux-switching machines.